JACS
JOURNAL OF THE AMERICAN CHEMICAL SOCIETY
Article
pubs.acs.org/JACS

Direct Pathway to Molecular Photodissociation on Metal Surfaces Using Visible Light

Emiko Kazuma,[†] Jaehoon Jung,[*,‡] Hiromu Ueba,[§] Michael Trenary,[∥] and Yousoo Kim[*,†]

[†]Surface and Interface Science Laboratory, RIKEN, Wako, Saitama 351-0198, Japan
[‡]Department of Chemistry, University of Ulsan, 93 Daehak-ro, Nam-gu, Ulsan 680-749, Republic of Korea
[§]Graduate School of Science and Engineering, University of Toyama, Toyama 930-8555, Japan
[∥]Department of Chemistry, University of Illinois at Chicago, 845 West Taylor Street, Chicago, Illinois 60607, United States

Supporting Information

ABSTRACT: We demonstrate molecular photodissociation on single-crystalline metal substrates, driven by visible-light irradiation. The visible-light-induced photodissociation on metal substrates has long been thought to never occur, either because visible-light energy is much smaller than the optical energy gap between the frontier electronic states of the molecule or because the molecular excited states have short lifetimes due to the strong hybridization between the adsorbate molecular orbitals (MOs) and metal substrate. The S−S bond in dimethyl disulfide adsorbed on both Cu(111) and Ag(111) surfaces was dissociated through direct electronic excitation from the HOMO-derived MO (the nonbonding lone-pair type orbitals on the S atoms (n_S)) to the LUMO-derived MO (the antibonding orbital localized on the S−S bond (σ^*_{SS})) by irradiation with visible light. A combination of scanning tunneling microscopy and density functional theory calculations revealed that visible-light-induced photodissociation becomes possible due to the interfacial electronic structures constructed by the hybridization between molecular orbitals and the metal substrate states. The molecule−metal hybridization decreases the gap between the HOMO- and LUMO-derived MOs into the visible-light energy region and forms LUMO-derived MOs that have less overlap with the metal substrate, which results in longer excited-state lifetimes.

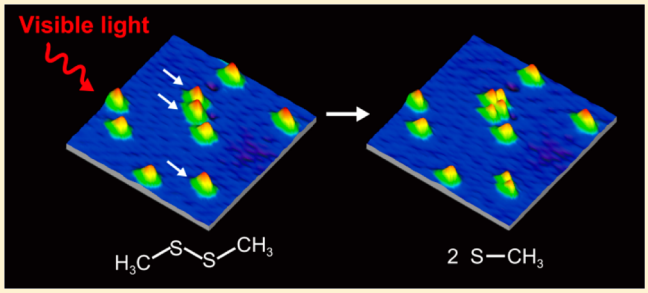

INTRODUCTION

Molecular photodissociation is a crucial reaction for the effective use of solar energy, a clean and renewable energy resource. However, the photodissociation of small molecules (H_2O, O_2, NO_x, SO_x, etc.) in the gas and liquid phases with visible light is not feasible because of the wide energy gap between the frontier molecular orbitals, such as the highest occupied molecular orbital (HOMO) and the lowest unoccupied molecular orbital (LUMO). Thus, although photodissociation has been studied extensively, most researchers have focused on irradiation by ultraviolet (UV) light. Molecular adsorption onto solid surfaces can provide a new opportunity for photochemical reactions with visible light, based on reconstructing the interfacial electronic structures due to the molecule−surface interaction. Visible-light-induced photodissociation has recently been achieved using both plasmonic noble metal[1−3] and nonplasmonic transition metal[4,5] nanoparticles, and these have attracted significant attention as a novel route to practical solar energy uses. Although a fundamental understanding of the relationship between the reaction profiles and the molecular electronic structure is crucial to elucidating the underlying mechanism of photodissociation on metal nanoparticles, the determination of the mechanism has been hampered by the nonuniform surface morphologies. In contrast, the atomically well-defined surfaces of metal single crystals enable both scanning tunneling microscopy (STM) and density functional theory (DFT) calculations to investigate the photoinduced surface dynamics and the accompanying changes in electronic structure necessary to obtain molecular-scale mechanistic insights.[6−8]

Molecular photochemistry of dissociation, desorption, and rearrangement, induced by UV light, on single-crystalline metal surfaces has been extensively studied.[9−17] The UV-light photodissociation of small molecules such as O_2,[9,10] Cl_2CO,[11] and OCS[12] has been observed even at low temperatures (30−100 K), although the excited states of the adsorbates on metal surfaces tend to relax rapidly (<100 fs).[18] Two excitation mechanisms, *indirect* (substrate-mediated) (Figure 1a) and *direct* (intra-adsorbate) (Figure 1b,c), have been proposed for the UV-induced surface dynamics of adsorbates on metal surfaces. In the *indirect* mechanism, hot electrons generated in a bulk metal by photoabsorption transiently enter the unoccupied states of the adsorbates through an inelastic scattering process,

Received: December 9, 2016
Published: February 7, 2017

DOI: 10.1021/jacs.6b12680
J. Am. Chem. Soc. 2017, 139, 3115−3121

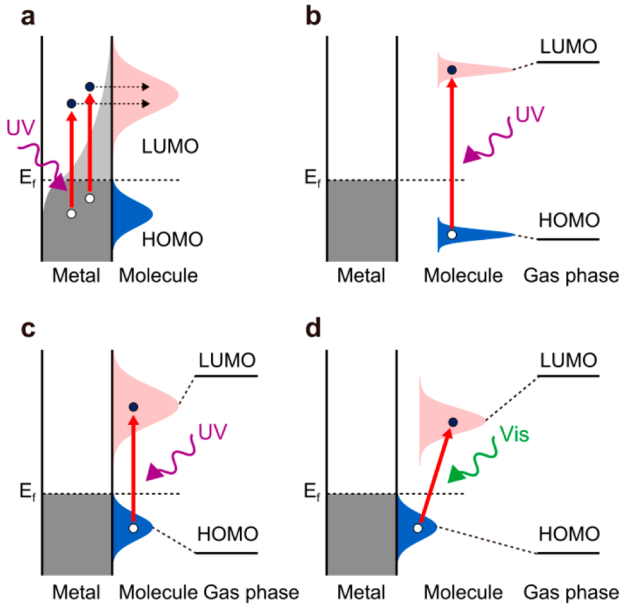

Figure 1. (a–c) Excitation mechanisms proposed for UV-induced photochemical reactions on metal surfaces. (a) Photodissociation through *indirect* (substrate-mediated) excitation. The hot electrons generated by photoabsorption in the bulk metal transfer transiently to the unoccupied states of the adsorbate molecule. The light gray area illustrates the distribution of the energies of the hot electrons. (b) Photodissociation through *direct* (intra-adsorbate) excitation of physisorbed molecules on a metal surface that has a HOMO–LUMO gap only slightly shifted from its gas phase value. (c) Photodissociation through *direct* excitation of chemisorbed molecules, in which the electronic states are strongly hybridized with the metal states. (d) Excitation mechanism for visible-light-induced photodissociation on metal surfaces. Photodissociation through *direct* excitation between the HOMO- and LUMO-derived MOs. The LUMO-derived MOs have negligible overlap with the metal substrate.

leading to the formation of ionic species that initiate photochemical processes.[19,20] The reaction probability is determined by the density of hot electrons in the metal substrate, and thus, the reaction yield depends on the photoabsorption spectrum of the metal.[16] Whereas *indirect* excitation is the primary pathway for photochemical reactions for numerous adsorbates on metal surfaces, only a few experimental observations have been attributed to the *direct* mechanism.[9,11,13−15] Photodissociation via the *direct* excitation of the frontier electronic states of an adsorbate on a metal substrate has been reported for physisorbed (Figure 1b) and chemisorbed molecules (Figure 1c). The sole example of photodissociation of a physisorbed molecule weakly interacting with a metal substrate is $Mo(CO)_6$ on Cu(111).[13] The wavelength dependence of the yield for that case is almost identical to the absorption spectrum of gas phase $Mo(CO)_6$, which implies that the incident UV light induces the *direct* excitation across the HOMO–LUMO gap of the adsorbed molecule. In contrast, chemisorbed systems show a photoexcited transition between the hybridized molecular orbitals (MOs) with a narrower energy gap than that in the gas phase due to the strong metal–adsorbate hybridization (Figure 1c). Only a few systems, such as O_2 on Pt(111)[9] and Cl_2CO on Ag(111),[11] have been investigated by means of temperature-programmed desorption after irradiation with UV pulse lasers. Notably, all previously reported photodissociation reactions on single-crystalline metal surfaces have been achieved only by excitation with UV light rather than with visible light, despite intense efforts to effectively utilize solar energy in photochemical reactions. This failure is either due to a wider molecular optical gap than the visible-light energy, or due to short lifetimes of the molecular excited states resulting from the strong hybridization with the metal surfaces. The real-space STM investigation of molecular photodissociation on metal surfaces, which has never been achieved, is essential to verify the mechanism.

In this paper, we report the visible-light-induced photodissociation of dimethyl disulfide, $(CH_3S)_2$, on Cu(111) and Ag(111) surfaces investigated by STM combined with DFT calculations. A quantitative analysis of the STM images revealed

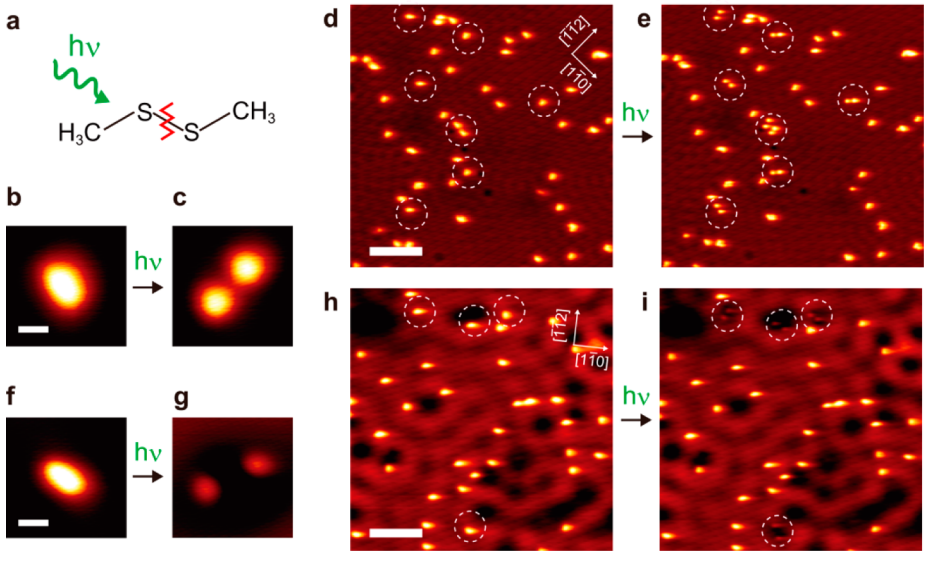

Figure 2. (a) Structure of a $(CH_3S)_2$ molecule, indicating the photodissociation of the S–S bond. (b–i) Topographic STM images of $(CH_3S)_2$ molecules on (b–e) Cu(111) and (f–i) Ag(111) observed at ∼5 K (V_{sample} = 20 mV and I_{tunnel} = 0.2 nA), (b, d, f, and h) before and (c, e, g, and i) after irradiation with 532 nm light (5.86×10^{16} photons cm^{-2} s^{-1}, 10 min). Dashed circles indicate dissociated molecules. The scale bars are 0.5 nm in panels b and f and 5.0 nm in panels d and h.

DOI: 10.1021/jacs.6b12680
J. Am. Chem. Soc. 2017, 139, 3115–3121

that S−S bond dissociation is induced by visible-light irradiation, unlike the gas phase photodissociation induced by UV light.[21−28] Moreover, the dissociation yield as a function of the wavelength of incident light indicates that the reaction is not induced by hot electrons generated in the photoexcited metal substrates but by *direct* excitation of the molecules with visible light. Furthermore, the DFT calculations reveal that hybridization between the molecule and metal reduces the energy gap between the frontier molecular electronic states derived from the HOMO and LUMO of $(CH_3S)_2$ in the gas phase, i.e., HOMO- and LUMO-derived MOs, resulting in an energy gap accessible with visible light. The LUMO-derived MOs, in particular, have negligible overlap with the metal surface, which keeps the lifetime of the photoexcited state long enough to induce photodissociation (Figure 1d). The hybridization between the molecule and the metal substrate opens a novel reaction pathway for molecular photodissociation on metal surfaces via *direct* excitation with visible light of the frontier MOs of the adsorbate. Our results on metal single crystals should apply to all forms of the bulk metal and will therefore be of more general applicability than results that pertain only to metal nanoparticles.

RESULTS AND DISCUSSION

Real-Space Observation of the Visible-Light-Induced Photodissociation of $(CH_3S)_2$ Molecules on Metal Surfaces. Photodissociation of isolated $(CH_3S)_2$ molecules (Figure 2a) adsorbed on Cu(111) was investigated by STM at a temperature of 5.0 K under ultrahigh vacuum (<4.0×10^{-11} Torr) conditions. An individual $(CH_3S)_2$ molecule adsorbed on Cu(111) appears as an elliptic protrusion in the STM images (Figure 2b), which agrees with previous observations of $(CH_3S)_2$ molecules on Cu(111).[29,30] Each molecule has a total of six equivalent adsorption orientations, reflecting the 6-fold symmetry of the Cu(111) surface.[29] The sample in the STM chamber was irradiated with light through a glass window, and during irradiation, the STM tip was retracted more than 2 μm from the sample surface to avoid influencing the adsorbates. Figure 2b−e shows the STM images obtained before and after irradiation with 532 nm light. After irradiation, some of the ellipsoids had broken into two identical ball-shaped protrusions (Figure 2c,e), implying the formation of two CH_3S molecules due to S−S bond dissociation. The remaining molecules retained their original shapes and orientations. The molecular photodissociation was observed to occur randomly within the light spot with a diameter of ∼1.2 mm. Control experiments in the dark showed that no dissociation occurs in the absence of light. It has been reported that the S−S bond of a single $(CH_3S)_2$ molecule on Cu(111) is dissociated to produce two CH_3S molecules through vibrational excitation of the S−S stretching mode by injecting tunneling electrons (>0.36 eV) from the STM tip.[30,31] The STM images taken after irradiation (Figure 2c) show two identical protrusions that have the same appearance as CH_3S molecules obtained by injecting tunneling electrons into a $(CH_3S)_2$ molecule. This indicates that S−S bond dissociation of $(CH_3S)_2$ on Cu(111) was induced by irradiation at 532 nm (2.33 eV). Notably, visible-light-induced photodissociation has not yet been observed in the gas and liquid phases, where much higher energy (∼5.0 eV) is required for dissociation of the S−S bond.[24−27]

The reaction ratio (N/N_0), which is defined as the number of $(CH_3S)_2$ molecules (N) after light irradiation divided by the total number of preadsorbed molecules (N_0), was measured to obtain quantitative information on the photodissociation reaction. Figure 3a shows the reaction ratio under light

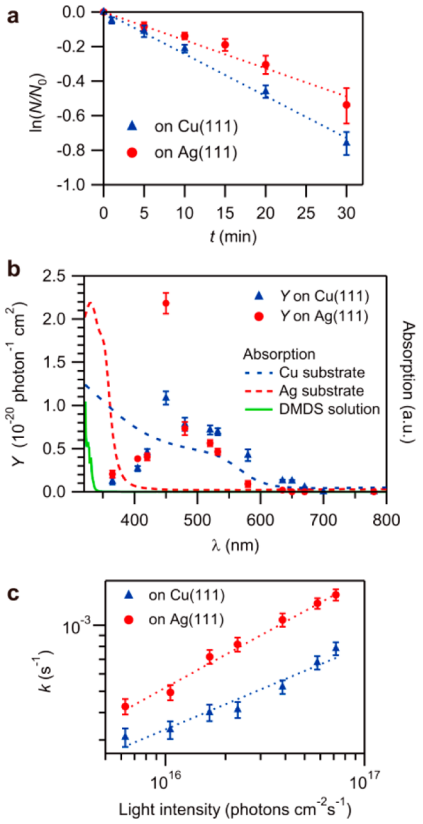

Figure 3. (a) Time dependence of the reaction ratio (N/N_0) for molecules on Cu(111) and Ag(111) under light irradiation at 532 nm (5.86×10^{16} photons cm^{-2} s^{-1}). Each data point is the average of 10 scan areas (30×30 nm^2), and the red and blue dotted lines are single exponential functions fitted to the data points ($\ln(N/N_0) = -kt$). (b) The wavelength (λ) dependence of the photodissociation yield (Y), which is the rate constant (k) divided by the number of incident photons per second. The blue and red dotted lines are the simulated absorption spectra of bulk Cu and Ag, respectively. The green line is the absorption spectrum of a $(CH_3S)_2$ solution. (c) Rate constant plotted against the intensity of 450 nm light.

irradiation at 532 nm as a function of the irradiation time (t). Each data point represents the mean value estimated from 10 scan areas (30 nm × 30 nm, $N_0 = 30 \pm 12$ per area) around the center of the light spot. The reaction ratio follows an exponential function, $\exp(-kt)$ (k: rate constant), because the dissociation reaction, $(CH_3S)_2 \rightarrow 2CH_3S$, is a first-order reaction. The reaction ratio follows the single exponential curve regardless of the time interval, indicating that the photodissociation of $(CH_3S)_2$ molecules on the Cu(111) surface is not induced by heat but by photons.

The photodissociation reaction of $(CH_3S)_2$ molecules was also examined by the irradiation of light with wavelengths (λ) ranging from 365 to 850 nm in the same manner as that used to obtain Figure 3a (Figure S1). The rate constant divided by the number of incident photons per second (A) (i.e., $Y = k/A$) is equivalent to the so-called photodissociation yield (Y), and we can, therefore, obtain the $Y-\lambda$ spectrum for the photodissociation reaction as shown in Figure 3b. The $Y-\lambda$ spectrum obtained on Cu(111) shows the peak and the threshold at ∼450 nm (∼2.76 eV) and at ∼670 nm (∼1.85 eV),

DOI: 10.1021/jacs.6b12680
J. Am. Chem. Soc. 2017, 139, 3115−3121

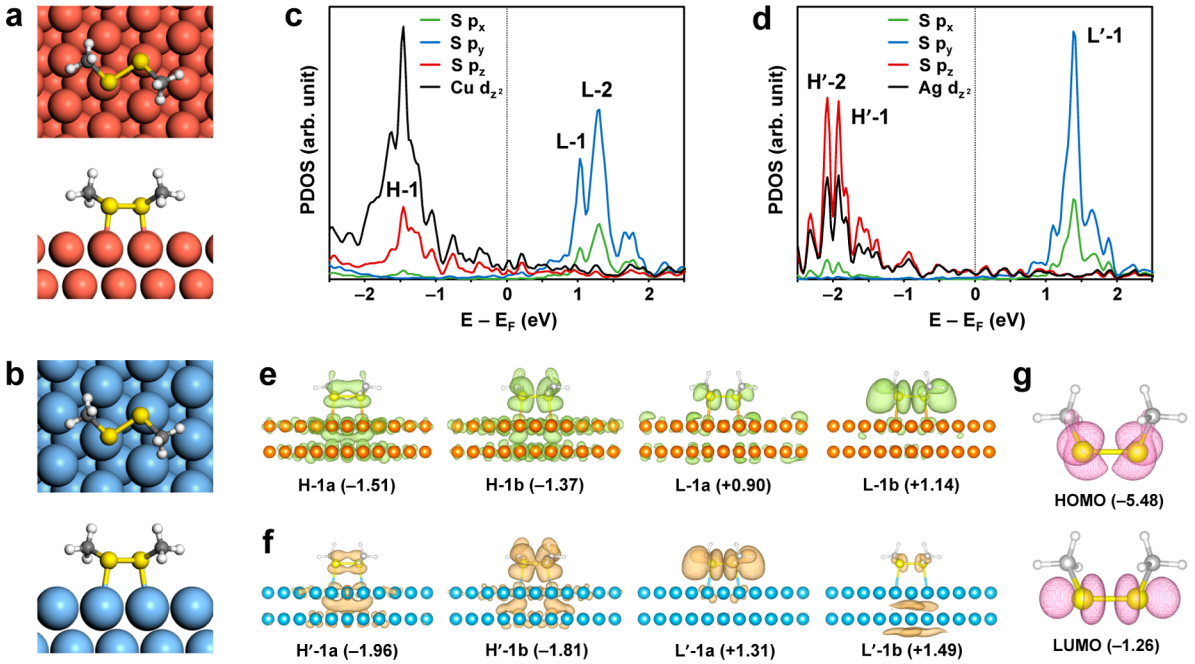

Figure 4. (a, b) The adsorption structures of a $(CH_3S)_2$ molecule on (a) Cu(111) and (b) Ag(111) optimized by DFT calculations. The *x*, *y*, and *z* directions are taken as parallel to the surface and perpendicular to the S–S pond, parallel to the surface and to the S–S bond, and perpendicular to the surface, respectively. (c, d) The calculated PDOS of three p-states on S atoms in a $(CH_3S)_2$ molecule and d_{z^2}-state of two metal atoms that are underneath the S atoms and directly interact with $(CH_3S)_2$ on (c) Cu(111) and (d) Ag(111). The zero energy corresponds to the Fermi level (E_F). The main DOS peaks for the frontier molecular electronic states are labeled H-1, L-1, and L-2 in panel c and H′-1, H′-2, and L′-1 in panel d. (e, f) The spatial distribution (isovalue = 0.0005 *e*/bohr^3) of the frontier orbitals nearest to E_F for an isolated $(CH_3S)_2$ molecule on (e) Cu(111) and (f) Ag(111) (magnified images of parts e and f including the electronic states for L-2 on Cu(111) and H′-2 on Ag(111) are provided in Figures S8 and S9). (g) The spatial distribution (isovalue = 0.01 *e*/bohr^3) of the HOMO and LUMO orbitals in the gas phase $(CH_3S)_2$.

respectively. Therefore, the photodissociation of $(CH_3S)_2$ molecules on the Cu(111) surface occurs in the visible-light wavelength region, which is much longer than the absorption tail for a $(CH_3S)_2$ solution measured with a UV–vis spectrophotometer (UV-3600, Shimadzu) (Figure 3b). This result implies that the photodissociation of $(CH_3S)_2$ molecules on the metal surfaces cannot be simply explained by the mechanism for physisorbed molecules shown in Figure 1b. In addition, if the reaction yield depends on the photoabsorption spectrum of the metal, it is reasonable to conclude that the reaction occurs by the *indirect* mechanism[16,19,20] (Figure 1a). However, the Y–λ spectrum does not follow the simulated photoabsorption spectrum of the Cu substrate, although it overlaps the visible region (Figure 3b).

If the photodissociation can be explained by the *direct* excitation mechanism for chemisorbed systems (Figure 1c), the reaction profile must depend on the frontier electronic states of the molecule hybridized with the metal substrate. Thus, we investigated the visible-light-induced photodissociation of $(CH_3S)_2$ molecules on a Ag(111) substrate, which has a different electronic structure from that of Cu(111). The STM images of $(CH_3S)_2$ molecules on the Ag(111) surface show a similar appearance with the same adsorption orientations as those on the Cu(111) surface (Figure 2f and Figure S2). The S–S bond dissociation of a single $(CH_3S)_2$ molecule adsorbed on Ag(111) was observed by injecting tunneling electrons at a sample bias higher than the threshold voltage of ~0.36 eV (Figure S3), indicating that the dissociation reaction with tunneling electrons occurs through vibrational excitation (see Supporting Information for details). The photodissociation of $(CH_3S)_2$ on Ag(111) was also achieved by irradiation with 532 nm light (Figure 2f–i), and the exponential dependence of the reaction ratio (N/N_0) on the irradiation time, which indicates a first-order reaction, was also observed (Figure 3a). The Y–λ spectrum has a sharper peak at ~450 nm (~2.76 eV) and a shorter threshold wavelength at ~635 nm (~1.95 eV) compared with the spectrum obtained on Cu(111) (Figure 3b). The Ag substrate exhibits no light absorption at wavelengths ≥450 nm,[32] so there is no overlap around the peak wavelength of the Y–λ spectrum on Ag(111) (Figure 3b). These results suggest that the visible-light-induced photodissociation of $(CH_3S)_2$ does not occur through excitation of the metal substrates (Figure 1a) but through direct excitation between the hybridized metal–adsorbate states.

The rate constant (k) at 450 nm, the peak wavelength in the Y–λ spectra (Figure 3b), increases linearly as the light intensity (I) increases, up to ~32 mW cm^{-2} (~7.2 × 10^{16} photons cm^{-2} s^{-1}) on both Cu(111) and Ag(111) (Figure 3c and Figure S4). The slopes (n's) of ln(k)–ln(I) plots are 0.55 ± 0.098 and 0.38 ± 0.080 on Ag(111) and Cu(111), respectively. If the photons reflected by the metal surface could be involved in the photodissociation reaction, then the resultant value "n" would be reduced from n = 1. The observed linear relationship clearly implies that the photodissociation of $(CH_3S)_2$ molecules on both surfaces does not occur through a thermal process. In addition, the thermal dissociation of $(CH_3S)_2$ on Cu(111) occurs at ~140 K,[33] which is much higher than the temperature of the substrate (~5.0 K). Note that the linear dependence of the reaction rate on light intensity also excludes indirect excitation with hot electrons (Figure 1a). For example, the dissociation rate of O_2 on Ag(110) with UV light increases exponentially with light intensity from ~0.5 × 10^{18} to 3.7 ×

DOI: 10.1021/jacs.6b12680
J. Am. Chem. Soc. 2017, 139, 3115–3121

10^{18} photons cm^{-2} s^{-1} because of the excitation of the substrate.[10] We thus conclude that visible-light-induced photodissociation of $(CH_3S)_2$ on the metal surfaces does not occur through the generation of hot electrons by excitation of the metal substrates (Figure 1a).

Electronic Structures of $(CH_3S)_2$ Molecules on Cu(111) and Ag(111). To verify the *direct* excitation mechanism, we carried out periodic DFT calculations (see the Methods section for computational details). The adsorption structures (Figure 4a,b) were optimized on the basis of the atomically resolved STM images. Two S atoms are located at the on-top sites of adjacent metal atoms, and thus, the molecular center is positioned above bridge sites on both surfaces (Table S1).[29,34] The adsorption energies of $(CH_3S)_2$ are 1.52 and 1.05 eV for the Cu(111) and Ag(111) substrates, respectively. Accordingly, the optimized distance between S and the nearest Cu atom (d_{S-Cu} = 2.34 Å) is shorter than d_{S-Ag} (2.66 Å). The direct interaction between S and the metal atoms underneath results in the elongation of d_{S-S} (Table S1), which would enhance the reactivity for S−S bond dissociation. In a comparison to d_{S-S} of $(CH_3S)_2$ in the gas phase, the d_{S-S} values on Cu(111) and Ag(111) increase by 0.08 and 0.06 Å, respectively.

The projected density of states (PDOS) and the spatial distribution of MOs for $(CH_3S)_2$ adsorbed on the metal substrates were investigated to examine the detailed electronic structures at the molecule−substrate interfaces. Figure 4c,d shows the PDOS of the three p-states of the S atoms and the d_{z^2}-state of the two metal atoms that are underneath the S atoms and that directly interact with $(CH_3S)_2$ on Cu(111) and Ag(111). On both surfaces, while the occupied molecular states are mainly composed of the S p_z-state, the unoccupied states are composed of S p_x and S p_y. The contribution of S p-states to the local DOS (LDOS) of $(CH_3S)_2$ indicates that the frontier states near the Fermi level (E_F) are mostly located at the two S atoms (Figure S5). In addition, the alignment of molecular frontier states with respect to the d-states of the metal substrates reveals that the occupied and unoccupied states of $(CH_3S)_2$ have extremely different characters in terms of interfacial hybridization (Figure S6). On the Cu(111) surface, the main peaks corresponding to the frontier states, i.e., the HOMO- and LUMO-derived MOs, of the $(CH_3S)_2$ molecule are located at ∼1.5 eV (peak H-1) below E_F and at ∼1.0 eV (L-1) followed by the peak at ∼1.4 eV (L-2) above E_F, respectively (Figure 4c). The H-1 aligns well with the d_{z^2}-state of the two Cu atoms underneath the S atoms (Figure 4c), but there is no significant distribution of the Cu s-, p-, and d-states in the unoccupied region (Figures S6 and S7). The charge density plots clearly represent the strong and weak interfacial hybridization between $(CH_3S)_2$ and Cu(111) at H-1 and L-1, respectively (Figure 4e). Both the H-1 and L-1 peaks consist of two overlapping electronic states at −1.51 eV (H-1a) and −1.37 eV (H-1b) and at +0.90 eV (L-1a) and +1.14 eV (L-1b). In a comparison of these with the frontier MOs of $(CH_3S)_2$ in the gas phase (Figure 4g), the H-1b- and L-1b-states have almost the same charge density distributions as the HOMO and LUMO of the gas phase $(CH_3S)_2$, respectively. The H-1a-state can be characterized by a π-bonding orbital along the S−S bond (π_{SS}), and H-1b is mainly composed of nonbonding lone-pair type orbitals on the S atoms (n_S). Both L-1a and L-1b are derived from the antibonding orbital localized on the S−S bond (σ^*_{SS}) isolated from the Cu(111) substrate. The PDOS (Figure 4d) and the spatial distribution of the charge density (Figure 4f) for the $(CH_3S)_2$ molecule on Ag(111) also exhibit an interfacial interaction similar to that on Cu(111). Two neighboring peaks in the occupied region, approximately −1.9 eV (H′-1) and −2.1 eV (H′-2), and one L′-1 peak in the unoccupied region (∼+1.4 eV), are observed. Figure 4e,f shows that both H′-1 and L′-1 nearest to E_F are composed of the same kinds of electronic states observed on Cu(111), although the relative stability of L′-1a and L′-1b is opposite to that of the corresponding states, L-1a and L-1b, on Cu(111). Therefore, as with the frontier states on Cu(111), the two states H′-1b and L′-1a on Ag(111) closest in energy to E_F can be characterized by n_S and σ^*_{SS}, respectively. The unoccupied frontier states with σ^*_{SS} character are electronically isolated from the substrate (Figures S6 and S7).

In the gas phase reaction, dissociation of the S−S bond of $(CH_3S)_2$ predominantly occurs with 248 nm (∼5.0 eV) light through the direct electronic excitation from n_S (HOMO) to σ^*_{SS} (LUMO) (Figure 4g).[21,24−27] Considering the remarkable similarity of the frontier states, H-1b (H′-1b) in the occupied region and L-1a (L′-1b) and L-1b (L′-1a) in the unoccupied region on the Cu (Ag) substrate, to the MOs of gas phase $(CH_3S)_2$, the photodissociation of the S−S bond on the metal surface also occurs through direct electronic excitation between the frontier electronic states ($n_S \rightarrow \sigma^*_{SS}$). In particular, the weakly hybridized electronic structure at the peak L-1 (L′-1) may provide an opportunity to extend the lifetimes of the excited states. Generally, the lifetime of an excited molecule adsorbed on a metal surface depends greatly on the degree of the interaction between adsorbate and metal substrate.[35−38] The lifetime of excitons for a C_{60} film on Au(111), for example, decreases from ∼350 fs with less than 30 monolayers to ∼80 fs with two monolayers because of the interactions between C_{60} and the metal substrate.[35] We thus conclude that the weak interactions between the frontier MOs of $(CH_3S)_2$ and the metal substrates, especially in the unoccupied region, extend the lifetimes of the excited states sufficiently to induce photodissociation (Figure 1d).

The computationally estimated energy gaps between the frontier electronic states for the expected excitation pathways ($n_S \rightarrow \sigma^*_{SS}$), i.e., H-1b → L-1a or L-1b on Cu(111) and H′-1b → L′-1a or L′-1b on Ag(111), are 2.27−2.51 eV (494−546 nm) and 3.12−3.30 eV (376−397 nm) on Cu(111) and on Ag(111), respectively. The numerical discrepancies between the energy gaps evaluated by DFT and the observed threshold energy of photodissociation might result from underestimating the adsorption strength of $(CH_3S)_2$ on coinage-metal substrates, even though we employed a density functional that accounts for dispersive interactions. However, the computational results not only describe well the reduction of the energy gap from the HOMO−LUMO gap of gas phase $(CH_3S)_2$ but also provide a way to explain the experimental results in which the threshold energy for photodissociation on Cu(111) was found to be lower than that on Ag(111) (Figure 3b). The reduction of the optical energy gap for an adsorbed molecule has been reported in the UV region.[39] Therefore, our results indicate that the hybridization between the molecules and the metal substrates reduces the energy gap between the frontier electronic states near E_F (Figure 1d), thus enabling photodissociation by visible light.

■ CONCLUSIONS

In conclusion, visible-light-induced photodissociation of the S−S bond in $(CH_3S)_2$ molecules adsorbed on Cu(111) and Ag(111) surfaces was investigated with STM combined with

DOI: 10.1021/jacs.6b12680
J. Am. Chem. Soc. 2017, 139, 3115−3121

DFT calculations on the PDOS and the spatial distribution of the frontier electronic states. Our work reveals that visible-light-induced molecular photodissociation on the metal substrates occurs through the direct excitation of the frontier states. The hybridization between $(CH_3S)_2$ and the metal substrate not only reduces the optical energy gap into the range of visible light, but also generates frontier states with less overlap with the metal substrate, opening a novel reaction pathway for the photodissociation by visible light of molecules adsorbed on metals.

METHODS

Experimental Details. The Cu(111) and Ag(111) substrates were cleaned using repeated cycles of Ar^+-ion sputtering and annealing at ~820 and ~860 K, respectively. The dimethyl disulfide, $(CH_3S)_2$, was degassed by freeze−pump−thaw cycles. The $(CH_3S)_2$ molecules were deposited by evaporation from a glass ampule at room temperature. The substrates were maintained at <50 K during deposition. The sample was transferred to a low-temperature STM (Omicron GmbH) maintained under ultrahigh vacuum (below 4.0×10^{-11} Torr). All STM measurements were performed at 5.0 K. The scanning conditions for obtaining STM images were V_{sample} = 20 mV and I_{tunnel} = 0.2 nA.

The light was *p*-polarized and introduced into the STM chamber through a view port (transmittance ≥95% at 365−1000 nm) with an incident angle of 25° to the sample surface. The light was collected by lenses outside of the chamber and concentrated on the sample surface with a spot diameter of ~1.2 mm. The UV-light source was a Hg lamp (SP-11, USHIO) equipped with a 365 nm bandpass filter (fwhm = 10 nm, THORLABS). The visible and near-infrared light sources were CW lasers (λ = 405, 450, 520, 532, 635, 650, 670, 780, and 850 nm, Collimated Laser Diode Module, THORLABS) and a Xe lamp (Laser-Driven Light Source, TOKYO INSTRUMENTS, INC) equipped with 420, 480, 580, and 700 nm bandpass filters (fwhm = 10 nm, THORLABS). The light intensity was tuned with an ND filter (THORLABS) and was evaluated with an optical power meter (THORLABS) and a dual scanning slit beam profiler (THORLABS).

DFT Calculations. Periodic DFT calculations were performed using the Vienna Ab-Initio Simulation Package (VASP) code[40,41] with Grimme's DFT-D3BJ[42,43] functional that accounts for the dispersive interactions. The core electrons were replaced by projector augmented wave (PAW) pseudopotentials,[44] expanded in a basis set of plane waves up to a cutoff energy of 400 eV. Large (6 × 6) supercells and a 4 × 4 × 1 Γ-centered k-point grid were used for its Brillouin zone sampling. The slab model consisted of six metal layers, with the two bottom layers fixed in their bulk positions during ionic relaxations. The periodically replicated slabs were separated by a vacuum region of ~18 Å, and the dipole correction was applied to avoid interactions between periodic slab images. The convergence criteria for the electronic self-consistent iterations and ionic relaxations were 10^{-7} eV and 0.02 eV/Å, respectively.

Simulation of Absorption Spectra. The absorption spectra of the Cu and Ag substrates were calculated on the basis of a finite-difference time-domain (FDTD) method via FDTD Solutions (Lumerical Solutions). The simulation model consists of a metal slab and a vacuum layer. The simulation domain consisted of 10 nm cubic cells, and the central region further meshed with a 3D grid of 1 nm spacing. The dielectric functions of Cu and Ag were extracted from data in the paper[45] and handbook,[46] respectively.

ASSOCIATED CONTENT

Supporting Information

The Supporting Information is available free of charge on the ACS Publications website at DOI: 10.1021/jacs.6b12680.

Figures S1−S9 and fractional coordinates of the optimized geometry for $(CH_3S)_2$/Cu(111) and $(CH_3S)_2$Ag(111) (PDF)

AUTHOR INFORMATION

Corresponding Authors

*jjung2015@ulsan.ac.kr

*ykim@riken.jp

ORCID

Michael Trenary: 0000-0003-1419-9252

Yousoo Kim: 0000-0001-7730-0704

Notes

The authors declare no competing financial interest.

ACKNOWLEDGMENTS

The present work was supported in part by a Grant-in-Aid for Scientific Research (A) [15H02025], Grant-in-Aid for Young Scientists (B) [16K17862], and RIKEN postdoctoral researchers (SPDR) program. This work was also partly supported by the National Research Foundation of Korea (NRF) grant [2015R1C1A1A01052947]. We are grateful for the use of the HOKUSAI-GreatWave Supercomputer system of RIKEN. M.T. acknowledges support from a grant from the US National Science Foundation (CHE-1464816).

REFERENCES

(1) Christopher, P.; Xin, H.; Marimuthu, A.; Linic, S. *Nat. Mater.* **2012**, *11*, 1044−1050.

(2) Mukherjee, S.; Zhou, L.; Goodman, A. M.; Large, N.; Zhang, Y.; Nordlander, P.; Halas, N. J.; Ayala-Orozco, C. *J. Am. Chem. Soc.* **2014**, *136*, 64−67.

(3) Kale, M. J.; Avanesian, T.; Christopher, P. *ACS Catal.* **2014**, *4*, 116−128.

(4) Sarina, S.; Zhu, H.; Xiao, Q.; Jaatinen, E.; Jia, J.; Huang, Y.; Zheng, Z.; Wu, H. *Angew. Chem., Int. Ed.* **2014**, *53*, 2935−2940.

(5) Kale, M. J.; Avanesian, T.; Xin, H. L.; Yan, J.; Christopher, P. *Nano Lett.* **2014**, *14*, 5405−5412.

(6) Bartels, L.; Wang, F.; Moller, D.; Knoesel, E.; Heinz, T. F. *Science* **2004**, *305*, 648−651.

(7) Comstock, M. J.; Levy, N.; Kirakosian, A.; Cho, J.; Lauterwasser, F.; Harvey, J. H.; Strubbe, D. A.; Fréchet, J. M. J.; Trauner, D.; Louie, S. G.; Crommie, M. F. *Phys. Rev. Lett.* **2007**, *99*, 038301.

(8) Bazarnik, M.; Henzl, J.; Czajka, R.; Morgenstern, K. *Chem. Commun.* **2011**, *47*, 7764−7766.

(9) Zhu, X. Y.; Hatch, S. R.; Campion, A.; White, J. M. *J. Chem. Phys.* **1989**, *91*, 5011−5020.

(10) Hatch, S. R.; Zhu, X. Y.; White, J. M.; Campion, A. *J. Phys. Chem.* **1991**, *95*, 1759−1768.

(11) Zhou, X. − L.; White, J. M. *J. Phys. Chem.* **1990**, *94*, 2643−2652.

(12) Kidd, R. T.; Lennon, D.; Meech, S. R. *J. Phys. Chem. B* **1999**, *103*, 7480−7488.

(13) Ying, Z. C.; Ho, W. *J. Chem. Phys.* **1991**, *94*, 5701−5714.

(14) Petek, H.; Weida, M. J.; Nagano, H.; Ogawa, S. *Science* **2000**, *288*, 1402−1404.

(15) Wolf, M.; Hotzel, A.; Knoesel, E.; Velic, D. *Phys. Rev. B: Condens. Matter Mater. Phys.* **1999**, *59*, 5926−5935.

(16) Zhu, X. Y.; White, J. M.; Wolf, M.; Hasselbrink, E.; Ertl, G. *Chem. Phys. Lett.* **1991**, *176*, 459−466.

(17) Liu, Z. M.; Costello, S. A.; Roop, B.; Coon, S. R.; Akhter, S.; White, J. M. *J. Phys. Chem.* **1989**, *93*, 7681−7688.

(18) Avouris, P.; Schmeisser, D.; Demuth, J. E. *J. Chem. Phys.* **1983**, *79*, 488−492.

(19) Frischkorn, C.; Wolf, M. *Chem. Rev.* **2006**, *106*, 4207−4233.

(20) Lindstrom, C. D.; Zhu, X. Y. *Chem. Rev.* **2006**, *106*, 4281−4300.

(21) Sheraton, D. F.; Murray, F. E. *Can. J. Chem.* **1981**, *59*, 2750−2754.

(22) Thompson, S. D.; Carroll, D. G.; Watson, F.; O'Donnell, M.; McGlynn, S. P. *J. Chem. Phys.* **1966**, *45*, 1367−1379.

(23) Bao, S.; Mcconville, C. F.; Woodruff, D. P. *Surf. Sci.* **1987**, *187*, 133−143.

DOI: 10.1021/jacs.6b12680
J. Am. Chem. Soc. 2017, 139, 3115−3121

(24) Boyd, D. B. *J. Am. Chem. Soc.* **1972**, *94*, 8799−8804.
(25) Lee, Y. R.; Chiu, C. L.; Lin, S. M. *J. Chem. Phys.* **1994**, *100*, 7376−7384.
(26) Rinker, A.; Halleman, C. D.; Wedlock, M. R. *Chem. Phys. Lett.* **2005**, *414*, 505−508.
(27) Luo, C.; Du, W.; Duan, X.; Liu, J.; Li, Z. *Chem. Phys. Lett.* **2009**, *469*, 242−246.
(28) Martínez-Haya, B.; Bass, M. J.; Brouard, M.; Vallance, C.; Torres, I.; Barr, J. *J. Chem. Phys.* **2004**, *120*, 11042−11052.
(29) Ohara, M.; Kim, Y.; Kawai, M. *Langmuir* **2005**, *21*, 4779−4781.
(30) Ohara, M.; Kim, Y.; Yanagisawa, S.; Morikawa, Y.; Kawai, M. *Phys. Rev. Lett.* **2008**, *100*, 136104.
(31) Motobayashi, K.; Kim, Y.; Ohara, M.; Ueba, H.; Kawai, M. *Surf. Sci.* **2016**, *643*, 18−22.
(32) Jiang, Y.; Pillai, S.; Green, M. A. *Opt. Express* **2015**, *23*, 2133−2144.
(33) Driver, S. M.; Woodruff, D. P. *Surf. Sci.* **2000**, *457*, 11−23.
(34) Fan, X.; Liu, Y.; Ran, R.; Lau, W. *J. Phys. Chem. C* **2013**, *117*, 6587−6593.
(35) Dutton, G.; Quinn, D. P.; Lindstrom, C. D.; Zhu, X. Y. *Phys. Rev. B: Condens. Matter Mater. Phys.* **2005**, *72*, 045441.
(36) Ino, D.; Watanabe, K.; Takagi, N.; Matsumoto, Y. *Phys. Rev. B: Condens. Matter Mater. Phys.* **2005**, *71*, 115427.
(37) Lindstrom, C. D.; Quinn, D.; Zhu, X.-Y. *J. Chem. Phys.* **2005**, *122*, 124714.
(38) Varene, E.; Bogner, L.; Bronner, C.; Tegeder, P. *Phys. Rev. Lett.* **2012**, *109*, 207601.
(39) Dixon-Warren, St. J.; Jensen, E. T.; Polanyi, J. C. *J. Chem. Phys.* **1993**, *98*, 5938.
(40) Kresse, G.; Hafner, J. *Phys. Rev. B: Condens. Matter Mater. Phys.* **1993**, *47*, 558−561.
(41) Kresse, G.; Furthmüller, J. *Phys. Rev. B: Condens. Matter Mater. Phys.* **1996**, *54*, 11169−11186.
(42) Grimme, S.; Antony, J.; Ehrlich, S.; Krieg, H. *J. Chem. Phys.* **2010**, *132*, 154104.
(43) Grimme, S.; Ehrlich, S.; Goerigk, L. *J. Comput. Chem.* **2011**, *32*, 1456−1465.
(44) Kresse, G.; Joubert, D. *Phys. Rev. B: Condens. Matter Mater. Phys.* **1999**, *59*, 1758−1775.
(45) Hagemann, H. J.; Gudat, W.; Kunz, C. *J. Opt. Soc. Am.* **1975**, *65*, 742−744.
(46) Lynch, D. W.; Hunter, W. R. *Handbook of Optical Constants of Solids*; Palik, E. D., Ed.; Academic Press: New York, 1985.

DOI: 10.1021/jacs.6b12680
J. Am. Chem. Soc. 2017, 139, 3115−3121